Optical In-Well Pumping of a Semiconductor Disk Laser With High Optical Efficiency

Svent-Simon Beyertt, Martin Zorn, Thomas Kübler, Hans Wenzel, Markus Weyers, Adolf Giesen, Günther Tränkle, and Uwe Brauch

***Abstract*—Optical in-well pumping is shown to lead to highly efficient operation of semiconductor disk-lasers using resonant absorption or using external optics. Pump radiation absorption of 70% at 940 nm is demonstrated for a laser emitting around 980 nm. Laser output power was 1.9 W with slope efficiencies up to 35% based on the incident power.**

***Index Terms*—InGaAs, optical pumping, quantum well, semiconductor disk laser, vertical external-cavity surface-emitting laser (VCSEL).**

I. Introduction

THE OUTPUT power of a single-mode vertical-cavity surface-emitting laser (VCSEL) is limited to some milliwatts. To further increase the output power the active area has to be enlarged which leads to disadvantages like multimode behavior as well as to problems using electrical pumping. To avoid multimode behavior an external cavity can be used instead of the top Bragg mirror, as it is demonstrated in the Novalux extended cavity surface emitting laser (NECSEL). However, homogeneous electrical pumping is still a challenge limiting the fundamental-mode output power of such a device to below 1 W [1], [2]. To get around this, optical pumping can be applied, leading to the so called vertical external cavity surface emitting laser (VECSEL), optically pumped semiconductor laser (OPSL) or semiconductor thin-disk laser. However, the absorption in the multi-quantum wells (QWs) forming the active region of usual semiconductor disk-lasers is very low. Therefore, Mooradian *et al.* used the barriers surrounding the QW as absorption layers [3], thus decoupling the pump radiation absorption from the QW absorption. This leads to relatively low spectral requirements for the pump diodes, because their wavelength only has to be shorter than the corresponding barrier material bandgap. Since the difference in the bandgaps of the QWs and the adjacent layers need to be sufficiently large, the minimal distance of pump wavelength to lasing wavelength is rather high, setting a lower limit for the quantum defect to typically 20%. In addition, for lasers emitting at shorter wavelengths it may be a problem to find appropriate pump lasers.

As we have reported previously [4], [5], for high quality materials, the quantum defect seems to have the biggest influence on the heat generated in the device. Therefore, minimizing the quantum defect is highly desirable, and can be done by direct optical pumping of the QWs [6]. This lead to the first demonstration of a continuous-wave (CW) semiconductor disk laser emitting 185 mW at 660 nm using the InGaAlP system [7]–[9]. Additionally, in-well pumping has been reported using GaAs QWs [10]. Within those experiments the pump light absorption was estimated to be 14%. To increase the absorption two methods can be applied. At first, a special optics can be used to realize multiple pump-beam passes through the semiconductor as in the solid-state disk lasers [11]. Second, one can use the cavity modes inside the structure, which arise from the subcavity formed by the air-semiconductor interface and the Bragg mirror, to enhance the absorption. Doing so, however, enhances the demand on the epitaxial process and on the pump diodes used, as now the pump wavelength has to coincide with one of the cavity resonances. The tolerances can be somewhat lowered if a combination of both methods is used.

II. Theoretical Background

A. Gain Medium

The principle of a semiconductor thin-disk laser is depicted in Fig. 1, with the details of the semiconductor structure being given in Fig. 2. In the simplest case—neglecting the pump source—it comprises two components only: an active mirror and a separate out-coupling mirror. The semiconductor active mirror is composed of a highly reflective Bragg mirror (DBR) followed by a stack of QW layers separated by spacer layers. A window layer on top of the chip prevents nonradiative surface recombination and surface oxidation. For optimal heat removal the active mirror is soldered directly with its Bragg side onto a heat sink.

B. Laser Equations

A simple rate-equation approach (1) is used to model the laser behavior neglecting all radial dependencies. Arbitrary but fixed laser wavelengths allow to compare the laser properties for different laser modes

$$\dot{n} = \eta_{\text{int}} \cdot W - c \cdot \frac{d_{\text{active}}}{L_{\text{res}}} \cdot g_{\text{eff}}(n) \cdot p - \frac{n}{\tau_{\text{tot}}(n)}$$
$$\dot{p} = \left[c \cdot \frac{d_{\text{active}}}{L_{\text{res}}} \cdot g_{\text{eff}}(n) - \frac{1}{\tau_{\text{cav}}} \right] \cdot p + \beta \cdot \frac{n}{\tau_{\text{rad}}(n)} \quad (1)$$

Manuscript received June 17, 2005; revised August 11, 2005. This work was supported in part by the Landesstiftung Baden-Württemberg GmbH of Stuttgart, Germany.

S.-S. Beyertt, T. Kübler, A. Giesen, and U. Brauch are with the Institut für Strahlwerkzeuge, Universität Stuttgart, 79569 Stuttgart, Germany (e-mail: simon.beyertt@ifsw.uni-stuttgart.de; kuebler@ifsw.uni-stuttgart.de; giesen@ifsw.uni-stuttgart.de; brauch@ifsw.uni-stuttgart.de).

M. Zorn, H. Wenzel, M. Weyers, and G. Tränkle are with the Ferdinand-Braun-Institut für Höchstfrequenztechnik (FBH), D-12489 Berlin-Adlershof, Germany (e-mail: zorn@fbh-berlin.de; wenzel@fbh-berlin.de; weyers@fbh-berlin.de; traenkle@fbh-berlin.de).

Digital Object Identifier 10.1109/JQE.2005.858794

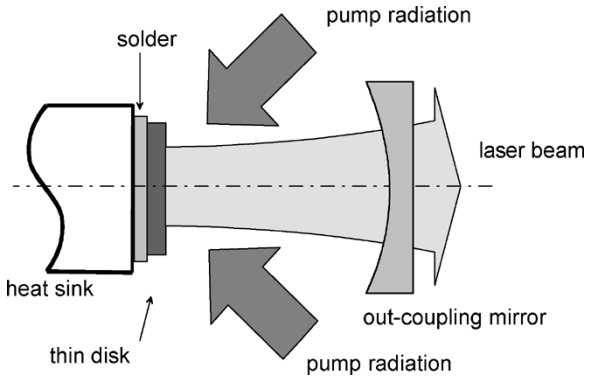

Fig. 1. Principle of the semiconductor thin-disk laser. The semiconductor structure (details shown in Fig. 2) is soldered onto a heat sink. The laser resonator is formed by the backside Bragg mirror and an external mirror. Pump radiation is focused quasi-longitudinally onto the disk.

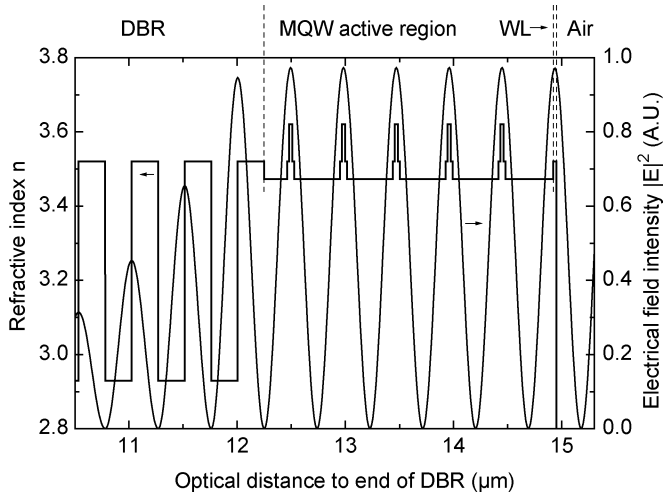

Fig. 2. Standard semiconductor structure consists of a MQW region grown on top of a distributed Bragg reflector (DBR). The QWs are separated by half of the design wavelength 980 nm. On top of the MQW a window layer (WL) is grown to prevent oxidation and non radiative recombination.

where n is here the charge carrier density, p the laser photon density, and W is the pump photon density given by $W = P_{\mathrm{abs}} \cdot (h \cdot \nu_{\mathrm{pump}} \cdot A_{\mathrm{pump}})^{-1}$, with $h \cdot \nu_{\mathrm{pump}}$ being the pump photon energy and A_{pump} the pump area. c is the speed of light, d_{active} the total thickness of the active area and L_{res} the total length of the resonator. $g_{\mathrm{eff}}(n)$ represents the effective gain of the material including standing-wave or cavity effects, which will be discussed in the following chapter. $\tau_{\mathrm{rad}}(n)$ represents the carrier lifetime for radiative transitions, $\tau_{\mathrm{tot}}(n)$ the total carrier lifetime (radiative and nonradiative), τ_{cav} the cavity lifetime and β the spontaneous emission factor (fraction of spontaneous emission emitted into the laser mode). The total carrier lifetime is assumed to be given by $\tau_{\mathrm{tot}}^{-1} = \tau_{\mathrm{rad}}^{-1} + \tau_{\mathrm{Auger}}^{-1}$, with the Auger lifetime being given by $\tau_{\mathrm{Auger}}^{-1} = C \cdot n^2$. For our calculations an Auger coefficient C of $6 \cdot 10^{-30}$ $\mathrm{cm}^6 \cdot \mathrm{s}^{-1}$ has been used, which is in the range of values published for GaAs and InGaAs [12], [13]. Impurity recombination, primarily relevant at low carrier densities, has been neglected.

An intrinsic efficiency η_{int} has been introduced taking into account that not every absorbed pump photon may generate a useful electron–hole pair. The intrinsic efficiency η_{int} equally increases the lasing threshold and reduces the differential efficiency. Another apparent reduction in differential efficiency is introduced if the pump area A_{pump} is larger than the laser-mode area A_{mode}. This defines the geometrical efficiency which can be approximated by $\eta_{\mathrm{geo}} \approx A_{\mathrm{pump}}/A_{\mathrm{mode}}$ assuming a homogeneous distribution of the carriers over the pumped area. Decreasing A_{mode} relative to A_{pump} decreases the differential efficiency but leaves the threshold density unchanged.

The differential quantum efficiency η_{diff} for small out-coupling values T is then given by

$$\eta_{\mathrm{diff}} = \eta_{geo} \cdot \eta_{\mathrm{abs}} \cdot \eta_{\mathrm{int}} \cdot \frac{T}{T+L} \cdot \frac{\lambda_{\mathrm{pump}}}{\lambda_{\mathrm{laser}}} \tag{2}$$

with L being the internal resonator loss, η_{abs} the absorption efficiency and $\lambda_{\mathrm{laser}}/\lambda_{\mathrm{pump}}$ the laser/pump wavelength, respectively. The heating of the device is included assuming a temperature rise proportional to the absorbed pump power. For each temperature and value of total loss $(T+L)$ the lasing wavelength leading to the maximum achievable output power is chosen. These wavelengths are subsequently used to calculate the whole temperature dependent output curve for a given heat sink temperature and out-coupling value.

Absorption, gain and photoluminescence (PL) spectra as well as the radiative lifetimes of the 8-nm InGaAs QWs used in the laser experiments have been calculated for various carrier densities n and temperatures T using a 8×8 $k \cdot p$ band model as described in [14]. Although many-body effects were neglected (except for phenomenological corrections for the gain spectral broadening and for the bandgap renormalization) good agreement with measurements was achieved [15].

C. Γ Factors

Inside the semiconductor a standing wave pattern of the electrical field exists originating from the external resonator and the additional intracavity Fabry-Pérot etalon given by the air-semiconductor interface and the Bragg mirror. Traditionally, standing-wave effects in VECSELs have been considered for the laser field only. There was no need to do so for the pump radiation when highly absorbing barrier layers were present. To take advantage of the standing waves, the QWs have to be placed at the antinodes of the standing wave pattern with a separation of $\lambda_{\mathrm{laser}}/2$ (see Fig. 2), which is usually called a resonant periodic gain (RPG) arrangement. In this way the intensity at the QWs is enhanced by the factor $\Gamma_{\mathrm{RPG}} = 2$ compared to the average intensity. The intensity is further enhanced by the internal cavity. Typically its length is carefully adjusted to the laser wavelength leading to a field intensity enhanced by the factor Γ_{cav}, determined by the reflectance of the mirrors forming the cavity and the absorption within that cavity. Together this results in an overall gain enhancement by a factor of $\Gamma_{\mathrm{RPG}} \cdot \Gamma_{\mathrm{cav}}$ at the laser wavelength, with typical enhancement values of seven times the intrinsic gain. The effective gain of the structure can then be written as

$$g_{\mathrm{eff}}(\lambda, \alpha) = \Gamma_{\mathrm{RPG}}(\lambda, \alpha) \cdot \Gamma_{\mathrm{cav}}(\lambda, \alpha) \cdot g_0(\lambda) \tag{3}$$

with $g_0(\lambda)$ being the intrinsic gain of the QWs (i. e., without cavity) calculated from $k \cdot p$ theory.

The situation becomes more complex in the case of resonant absorption, where Γ_{RPG} and Γ_{cav} are to be optimized for both the pump and laser fields. To accomplish this, the laser has to be designed so that the antinodes of both the laser radiation and the pump radiation lie at the locations of the QWs. Because the periodicity of the standing wave pattern along the cavity axes is given by $\lambda_{\mathrm{SW}}(\alpha', \lambda) = \lambda/\cos(\alpha')$ the antinodes of the two fields can be brought into alignment by adjusting the internal angle of incidence α' of the pump radiation λ_{pump}. Therefore, if the structure is resonant for the laser field at normal incidence, to bring the pump in resonance requires $\lambda_{\mathrm{SW}}(0°, \lambda_{\mathrm{laser}}) = \lambda_{\mathrm{SW}}(\alpha', \lambda_{\mathrm{pump}})$, leading to

$$\lambda_{\mathrm{pump}} = \lambda_{\mathrm{laser}} \cdot \cos(\alpha'). \tag{4}$$

This leads to enhanced absorption as well as to enhanced gain. When calculating α', one has to take into account that the corresponding external angle α is much larger due to a typical refractive index of 3.5. For resonant pumping the bleaching of the absorption limits the minimal difference between pump and laser wavelength. A difference of -30 nm already requires an external angle α of 70° and thus this approach requires a pump beam with good quality in the plane of incidence. A positive side effect of the large angles involved is the increased Fresnel reflectance for the s polarization and with that the increased Q of the internal resonator. This leads to a higher field enhancement inside the cavity which further enhances the absorption on resonance (in our example with 13 QWs to a remarkable 90% at low pump-power densities).

Unfortunately, the highly divergent, unpolarized and spectrally broad beam of a typical fiber-coupled diode-array pump source neither allows for such large pump angles (4) nor does it allow to use a narrow resonance. Therefore, a different resonance for pumping and lasing has to be used, and one has to determine the dependence of field intensity $|E|^2$ at the QW positions on the angle of incidence as well as on the wavelength. The spectral position of the cavity modes as well as the position of the Γ_{RPG} maxima for different angles of incidence is easily calculated using (4). However, the amplitude of the cavity resonances strongly depends on the amount of surface reflectance, given by the Fresnel formula, and thus depends on polarization state and angle of incidence.

Fig. 3 shows the calculated $\Gamma(\lambda)$ functions for a standard active-region design with 12 QWs positioned at the antinodes of the laser field (for a wavelength of 980 nm). The electrical-field distribution has been calculated using a commercial multilayer-mirror design program (Spektrum, LZH Hanover). For simplicity the active area is considered to be lossless leading to a constant amplitude of the standing wave inside the structure. In this approximation Γ_{cav} is given by $n|E|^2(n_0|E_0|^2)^{-1}$, with n being the refractive index inside, n_0 the one in front of the structure, and E (E_0) the corresponding field amplitudes. $\Gamma_{\mathrm{RPG}}(\lambda)$ is then given by [16]

$$\Gamma_{\mathrm{RPG}} = \frac{L_{\mathrm{cav}}}{d_{\mathrm{active}}} \cdot \frac{\int\limits_{\mathrm{active}} |E(z)|^2 \, dz}{\int\limits_{\mathrm{cavity}} |E(z)|^2 \, dz} \tag{5}$$

with L_{cav} being the thickness of the internal cavity.

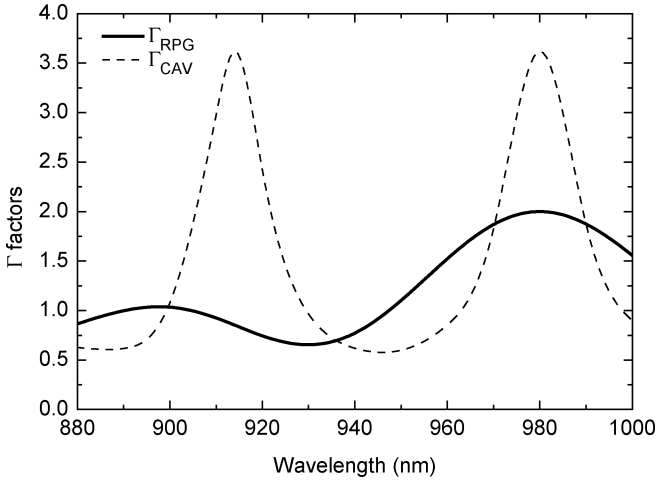

Fig. 3. Γ_{RPG} (solid) and Γ_{cav} (dashed) factor calculated for of a structure with 12 RPG periods and a cavity length of 25 $\lambda/4$ optimized for $\lambda = 980$ nm using the Spektrum software. The cavity mode spacing is smaller than the spacing between the maxima of Γ_{RPG} resulting in nonideal pump absorption for the cavity mode at 914 nm.

As can be seen in Fig. 3, $\Gamma_{\mathrm{cav}}(\lambda)$ repeats its maximum at the next cavity mode(s) with an amplitude depending on the cavity Q factor at that wavelength. Within the Bragg-mirror stopband $\Gamma_{\mathrm{RPG}}(\lambda)$ possesses only one maximum at 980 nm since at all other wavelengths there are some antinodes that are away from the corresponding QW.

However, having selected one of the cavity resonances for pumping, Γ_{RPG} is easily optimized by moving those QWs that would be close to a field minimum of the pump radiation to positions with still good overlap for both laser and pump field. Keeping the cavity thickness constant (Γ_{cav} unchanged) this can be done by using more than one QW per antinode or by reducing the overall number of QWs.

D. Temperature Effects

For an optimum operation of the device at a given laser wavelength λ_{laser}, the intrinsic gain g_0 as well as Γ_{RPG} and Γ_{cav} should reach their maximal values at the working point, defined by the pump power (density), output coupling, and device temperature. Since the intrinsic gain on the one hand and the RPG and cavity resonances on the other hand possess different temperature coefficients of roughly 0.3 and 0.1 nm/K, respectively, the device can be designed for one working point only with a usually sharp roll-over at higher pump powers due to the decreased effective gain. In contrast to spacer pumping the absorption is additionally reduced at elevated temperatures because of the detuning between cavity mode used for resonant pumping and pump laser wavelength. This makes it necessary to adjust the pump wavelength to the pump resonance position for the given working point. With antireflective (AR) coating for the lasing wavelength, the thermal roll-over should be smoother as the laser is not bound to the cavity resonance, and can, therefore, tune more freely to the intrinsic gain maximum. However, for resonant absorption to be still effective the surface reflectance for the pump radiation should remain at values higher than 30% making multilayer dielectric coatings necessary.

E. Photoluminescence (PL)

The gain of the QWs normal to the surface is quite small and it is, therefore, difficult to be measured precisely. In order to verify the calculated gain curves on which the entire laser modeling relies, a loophole is to measure the PL instead and compare this to the calculated PL. Considering the spontaneous emission as being stimulated by the vacuum field which is modified by the cavity, it is clear that basically the same considerations concerning the cavity effects apply as for the stimulated emission/absorption. This has already been noticed by Purcell in 1946 [17]: The spontaneous radiative transition rate along the optical axis of a cavity is changed if the density of optical modes $\rho(\nu)$ is altered from its value of $2n/c$ for a homogeneous one-dimensional medium [18]. The photo emission from the cavity is, therefore, given by

$$I_{\mathrm{QW}}(\lambda,\alpha) \propto \Gamma_{\mathrm{RPG}}(\lambda,\alpha)\cdot\Gamma_{\mathrm{cav}}(\lambda,\alpha)\cdot|\mathrm{WP}(\lambda,\alpha)| \quad (6)$$

with $\mathrm{WP}(\lambda,\alpha)$ being the intrinsic emission profile of the QWs, i.e., the spectrum of the radiation emitted from the QW in the absence of the cavity. The width of the cavity resonances is typically much smaller than the width of $\mathrm{WP}(\lambda,\alpha)$, leading to strong emission lines at the cavity-resonance wavelengths. Using the angular or temperature shift of the cavity resonances, the resonance can be swept across the emission profile $\mathrm{WP}(\lambda,\alpha)$. When determining the intrinsic emission from such measurements one has to take into account the angular dependence of Γ_{cav} and Γ_{RPG} as well as the angular and temperature dependence of the intrinsic emission. To circumvent this, the intrinsic emission could be alternatively determined from AR coated samples or from the PL emitted from the edges of the sample.

III. Experimental Results

A. Sample Preparation

The semiconductor structures were grown by metal–organic vapor-phase epitaxy (MOVPE) in an Aixtron AIX 200/4 reactor on 2-in GaAs (100) substrates misoriented 2° toward the nearest (1–10) plane [19]. They consist of a buffer with an etch-stop layer, an active region and a binary AlAs–GaAs 25 period Bragg mirror with its stopband centered at 980 nm. Since the structures are designed as bottom emitters, the active region has to be grown before the Bragg mirror. After the GaAs buffer layer an InGaP etch-stop layer is grown to allow for later substrate removal. Then 13 $In_{0.15}Ga_{0.85}As$ single QWs (SQWs) with 8 nm thickness for emission at 980 nm (bandgap at 1.26 eV) are placed in the antinodes of the electrical field at 980-nm emission perpendicular to the layer. They are surrounded by compositionally graded $Al_xGa_{1-x}As$ barriers with x increasing from 0% to 20% (bandgap from 1.424 eV to 1.673 eV) which include strain compensation by $Al_{0.2}Ga_{0.8}As_{0.8}P_{0.2}$. All layers are undoped to minimize absorption losses. A standard metallization is then evaporated onto the epi-side of the wafers to allow for soldering. After that they are sawn into 2×2 mm^2 chips which are then soldered onto CuW heat spreaders using Au–Sn hard solder [20]. The chips are then glued to a glass carrier and the substrate is etched off wet-chemically. The InGaP etch-stop provides a smooth surface of the remaining semiconductor film of only 6 μm thickness. After substrate removal the submounts are removed from the glass carrier and soldered to a copper plate.

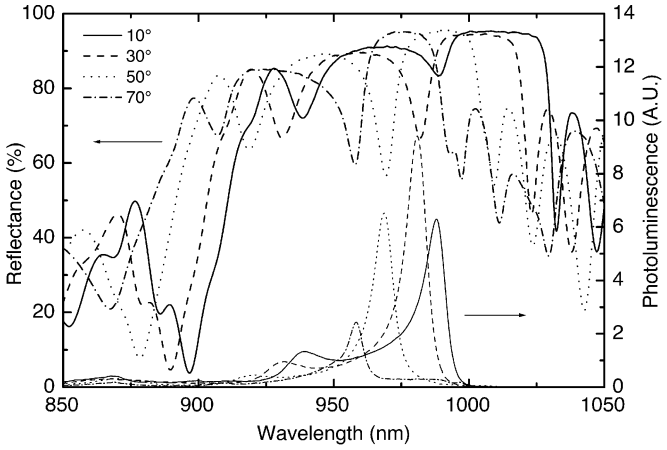

Fig. 4. Measured reflectance (left ordinate) and PL spectra (right ordinate) for different angles at a heat-sink temperature of 20 °C. The Bragg mirror stopband shows a break-in due to the enhanced absorption on resonance. The same cavity resonance also affects the PL emitted into that angle. Increasing the measuring angle shifts the resonances as well as the stopband to shorter wavelengths.

B. Spectroscopy

1) Experimental Setup: The reflectance spectra were recorded using a halogen lamp with the pin-hole in front of the lamp imaged onto the sample to give a spot size of approximately 500 μm. The reflected radiation is then imaged onto the multimode fiber of a CCD spectrometer (StellarNET, EPP2000, 800–1200 nm, 0.8 nm resolution). An aperture limits the numerical aperture (NA) on the sample to 0.05 to provide high angular resolution. For geometrical reasons the smallest reflection angle that can be measured is 10°. The reference spectrum is recorded in an 180° arrangement with the sample holder removed. Due to variations in the coupling efficiency of the light into the spectrometer fiber, the absolute value of the measured reflectance has an error of approximately 5%. For PL measurements the light of the halogen lamp is blocked and the 5-mW 780-nm radiation from a small diode laser is focused at an angle of 45° onto the same spot instead. In both cases the sample temperature is controlled using a thermo-electric cooler (TEC).

2) Experimental Results: The reflectance spectra of the uncoated sample recorded for different angles of incidence α (Fig. 4) allow to determine position and strength of the resonances for pumping and lasing as well as the position of the Bragg mirror. For 10° two dips at 990 and 940 nm corresponding to two cavity modes within the Bragg-mirror stopband (920–1030 nm) can be seen. With increasing α, the stopband as well as the resonances, move to shorter wavelengths. As expected, the same resonances can be seen in the PL spectra (also shown in Fig. 4). Changing the heat sink temperature allows to analyze the temperature shifts. Both, the cavity resonances and the Bragg mirror stopband shift with 0.07 nm/K.

3) Γ Factors: For modeling the real Γ functions have to be known. Comparing the measured reflectance spectra with the spectra calculated with the nominal layer design data (software:

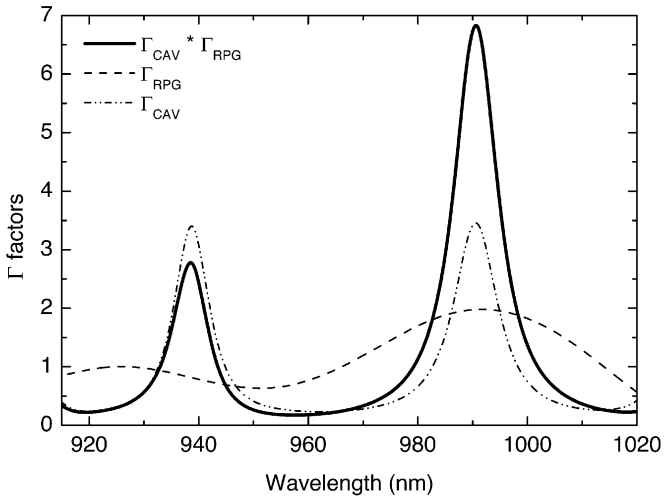

Fig. 5. Γ_{RPG} and Γ_{cav} factors of the laser sample for normal incidence together with the product of both calculated using the Spektrum software. The nominal layer-design data have been slightly modified to fit the calculated to the measured reflectance spectra (Fig. 4).

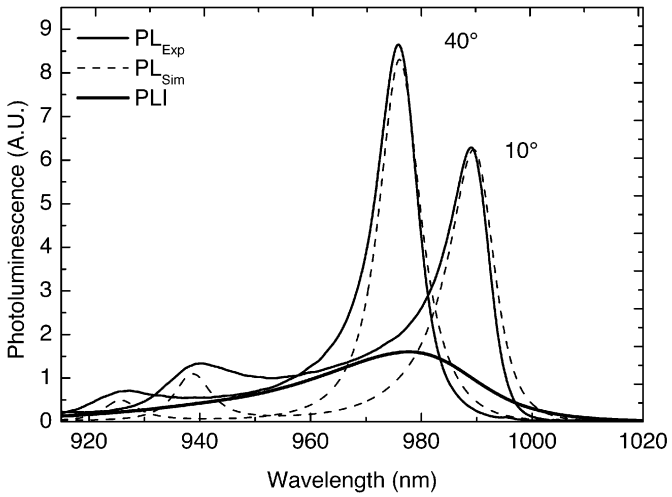

Fig. 6. Calculated PL spectra for 10° and 40° (dashed lines) using the Γ factors of Fig. 5 and the calculated intrinsic PL (solid, bold line). Also shown is the corresponding measured PL (solid line).

Spektrum, data base: SOPRA) allows to fine-adjust the thickness of the etch-stop, spacer and the Bragg layers to match the position of the reflection peaks and to calibrate the transition strength of the QW absorption. The best fit could be achieved with an RPG period of 995 nm, a Bragg period of 980 nm, and a thinner than designed etch-stop layer which varied on the samples from the center to the edges. Assuming a small wavelength-independent absorption α_{test} for the QWs and using the actual layer composition of the sample the Γ functions can be easily calculated. This could be done because the cavity is far from being impedance matched—which would be the case for $\sqrt{R_1} = \sqrt{R_2} \cdot V_0$ with $V_0 = \exp(-\alpha_0 L)$—and, therefore, the Γ factors are approximately independent of the intrinsic gain or absorption. Then the effective gain of the structure can be written as given in (3).

This is correct as long as all QWs experience the same field, e.g., if they are perfectly matched to the standing wave, forming an ideal RPG structure. In all other cases one gets only an averaged value for gain and absorption. The so calculated Γ functions (near the sample center, used for diode pumping) are shown in Fig. 5. The cavity resonance at 990 nm matches nicely the RPG resonance, resulting in a combined Γ factor of almost 7 at 990 nm. In order to verify the spectral position of the (calculated) transition as well as the Γ factors determined from the reflectance spectra, the calculated (intrinsic) PL spectra (at low carrier density; maximum near 980 nm) are multiplied by the combined Γ factor of Fig. 5. The resulting cavity-enhanced PL together with the measured PL is shown in Fig. 6 for observation angles of 10° and 40° with the calculated intrinsic PL also shown for comparison. At the resonance positions the agreement is quite satisfactory while the observed off-resonance suppression of the PL is not as strong as calculated.

It is evident that even for large pump angles (70°) the angle-shifted laser resonance can only be used for pumping near the edges of the sample where the resonance is shifted from 960 to 940 nm at 70° (corresponding to a resonance position of 972 nm at normal incidence). Only then, the distance to the PL maximum is sufficiently large to get an effective absorption of the pump radiation under lasing conditions. With s polarized pump radiation a combined Γ factor of 13 can be expected. For diode pumping, where such large pump angles are not feasible, the next cavity resonance has to be used. Unfortunately, this is positioned near a minimum of Γ_{RPG}, reducing the combined Γ factor to below 3 on resonance. Additionally, for our experiments where the angle of incidence is fixed at 30° the pump-diode wavelength of 940 nm is off by 10 nm from the cavity resonance, further reducing the possible Γ factor from 3 to below 1.

TABLE I
DETAILS OF THE THREE PUMP SETUPS USED IN THE EXPERIMENTS

set-up	# 1	# 2	# 3
pump laser	Ti:sapph.	Diode	Diode
wavelength (nm)	780–940	800	938
power (W)	3	20	17
pump spot (μm)	100–150	250–300	300
reimaging	1 x	0 x	11 x
pump angle (°)	70	30	28
NA	0.05	0.15	0.15
polarization	s	none	none

C. Laser Performance

1) Experimental Setup: For the laser experiments approximately semiconcentric resonators with mirror radii of 50 or 150 mm were used. The resonator length was adjusted to give the maximum possible output power leading to multimode emission of the samples. Three different setups for pumping have been used (details are listed in Table I). The Ti:sapphire pump laser allows for fitting the pump wavelength to the resonance structure and to directly compare spacer and QW pumping. To increase the absorption efficiency the pump radiation is reimaged once onto the pump spot. Fiber-coupled diode laser arrays are used for high-power spacer and QW pumping.

For spacer pumping a fiber coupled diode-laser array emitting 20 W at 800 nm from a 200-μm NA-0.2 fiber was used.

The fiber end was imaged onto the sample with a magnification factor of 1.4 at an angle of incidence of 30°, resulting in an elliptical pump spot of 307 μm $\times$ 275 μm [full-width at half-maximum (FWHM) of a super Gaussian power-density distribution]. For QW pumping, a diode-laser array emitting 17 W at 938 nm from a similar fiber was used. With the high-NA pump beam only pump angles between 30° and 50° can be applied, which prevents to fit the pump angle to a strong resonance as in the case of Ti:sapphire pumping. To compensate for the relatively small single-pass absorption a multi-pass pump optics (originally designed for an Yb: YAG thin-disk laser) was used. Here, various segments of a parabolic mirror are applied to image the fiber end 12 times along various planes of incidence onto the sample. To reach a pump spot of 300 μm, the beam had a relatively large cross section resulting in high transmission losses of the multi-pass optics of 30%–40% with a high-reflective (HR) mirror replacing the sample. The beam transforming optics had a transmission of only 70% resulting in about 12 W of pump power entering the multi-pass pump optic. This is not a principal problem, but it increases the uncertainty in the absorbed-pump-power measurement when using the multi-pass optics. For all experiments the incident, the reflected and the laser output power were recorded simultaneously. From this, the power deposited within the sample was calculated. For the QW pumped case the DBR has still a high reflectance ensuring that all absorbed power is absorbed within the QWs. For spacer pumping approximately 15% of the absorbed pump power is lost into the DBR making it necessary to correct the measured absorbed power by that factor. For every data point a PL spectra was recorded giving the possibility to analyze the spectral shift of the resonances as well as the laser wavelength with its absorbed power. Together with the spectral shift of the cavity resonances as function of temperature, this gives a measure of active-region temperature.

2) Ti:sapphire Pumped: The high beam quality of the Ti:sapphire laser has several advantages over diode-array pumping despite its limited output power: Pump spots with diameters of 100 μm and smaller are possible, allowing high pump-power densities and improved cooling efficiency due to a more pronounced three-dimensional (3-D) heat flux. The low-divergent, polarized beam allows to use large angles of incidence and s polarization to maximize the resonant absorption. In addition, the laser can be tuned to match exactly one of the resonances for QW pumping or alternatively to match the absorption band of the spacer layers for spacer pumping to directly compare the respective laser efficiencies.

Fig. 7 shows the output powers versus the absorbed pump powers for spacer and QW pumping, respectively, for different output couplings. The position of the pump spot—near one of the edges—has been optimized for QW pumping into the laser resonance at 940 nm. The same pump spot was later used for QW pumping at 892 nm (which corresponds to the next cavity resonance) and for spacer pumping at 800 nm. Increasing the out-coupling from 0.8% to 2.8% only slightly increases the slope, indicating that the resonator losses are of the order of 0.2%. The slope of 48% for 2.8% out-coupling and 940 nm QW pumping is almost twice as high as for spacer pumping (27%), the threshold is 30% lower, which is slightly more than

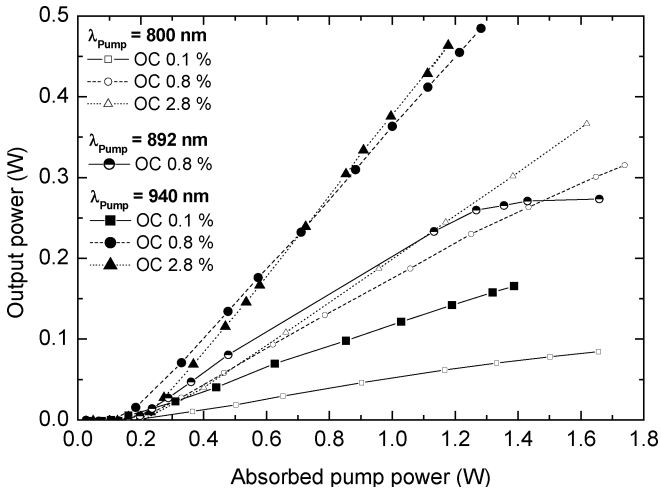

Fig. 7. Output power versus absorbed pump power for spacer and QW pumping, respectively, using the Ti:sapphire pump setup #1 and out-coupling values of 0.8%, 1.5%, and 2.8%. Pumping directly into the angle-shifted laser resonance shows the best performance due to the very homogeneous excitation of the QWs. Pumping the next cavity mode or the barriers results in more inhomogeneous pumping and thus in a reduced device performance.

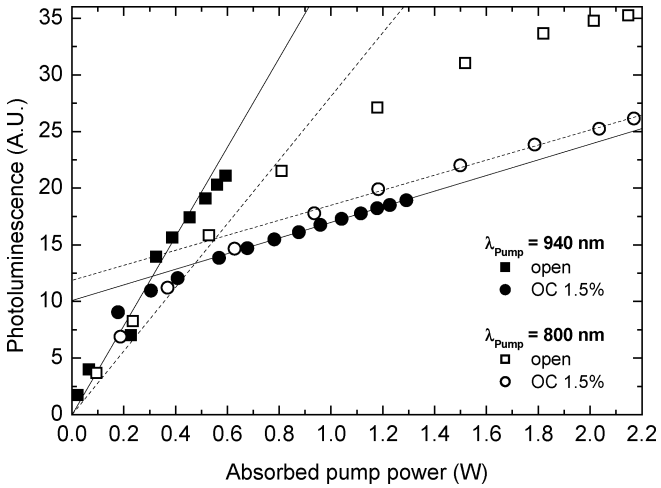

Fig. 8. Integrated PL for spacer (open symbols) and QW pumping (filled symbols) with (circles) and without (squares) external resonator using the Ti:sapphire pump source and pump setup #1. With resonator the integrated PL signal shows a reduced slope after lasing threshold, but even without resonator the PL signal saturates at higher pump powers due to the onset of nonlinear effects.

what is expected from the reduced quantum defect (-15%) alone. Although spacer pumped the spontaneous emission is somewhat enhanced below 900 nm, the integrated spontaneous emission during laser operation is only 10% stronger. This is mainly due to the higher spacer-pumped threshold (Fig. 8). The output characteristics for 892-nm QW pumping (slope 24% for 0.8% out-coupling) are more like those for 800 nm spacer pumping than those for 940 nm QW pumping. Common to the 892- and 800-nm pumping cases are the inhomogeneously pumped QWs. The former due to the misfit of the RPG period, the latter due to Lambert–Beer's law, both leading to an increase in threshold [21].

Without lasing (the resonator being blocked) one would expect the integrated PL to increase linearly with the absorbed pump power. Experimentally one finds a strongly reduced slope for pump powers twice or triple the threshold pump power

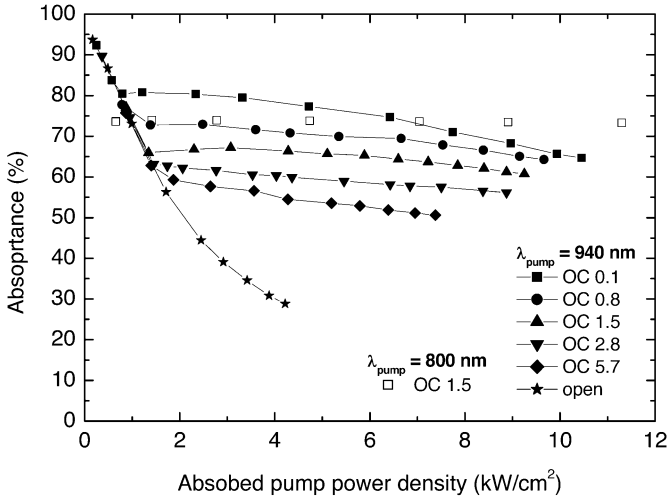

Fig. 9. Pump absorption versus pump power density for spacer (open symbols) and QW pumping (filled symbols) using the Ti:sapphire pump setup #1 and various out-coupling values. Without laser resonator (stars) there is a strong bleaching of the absorption transition. With laser resonator the absorption "clamps" at the value defined by the threshold density of the QWs.

(Fig. 8), i.e., increased nonradiative transitions like Auger recombination occurs. When lasing the PL should be clamped at its threshold value, experimentally, however, it still increases with a reduced slope. This is a result of the imperfect overlap between pump and laser mode and an increasing threshold with pump power and, hence, device temperature. Only the PL emitted out of the laser mode area should be clamped at its threshold value, whereas the PL emitted out of the remaining pumped area will increase like in the non-lasing case. Together this gives a reduced slope for the integrated PL above lasing threshold and thus a measure for the possible amount of misfit η_{geo} between pump and laser mode. This is also consistent with a slight decrease of the pump absorption above threshold which is otherwise nicely clamped at its threshold value (Fig. 9). Reimaging the pump radiation once gives an absorption efficiency of 65%–70% with 0.8% out-coupling, decreasing to 55%–50% with 5.7% out-coupling, making the 0.8-% out-coupler the better choice in terms of overall laser efficiency. Without lasing the absorption at 940 nm decreases with 25% /(kW/cm^2), indicating a transparency density of 4 kW/cm^2 at the pump wavelength. The nonlinearity for higher pump power densities may be attributed to Auger recombination or additional absorption which does not contribute to the carrier density—either in the pump optics or in the sample.

3) Diode-Laser Pumped: Diode pumping allows for the increase of absorbed pump power approximately fivefold at constant pump power density. Due to the increased pump spot size the cooling is now less effective because of the reduced 3-D heat-spreading effect. The output power as function of the absorbed pump power is shown in Fig. 10(a) for both QW and spacer pumping. The corresponding power densities are shown in Fig. 10(b), together with the 940-nm pumped Ti:sapphire results for comparison. For an out-coupling of 2.7% a slope efficiency of 35% for in-well pumping and 30% for spacer pumping is achieved. This compares nicely to the in-well pumped Ti:sapphire results of 24% (892 nm) and 48% (940 nm), taking into account that the Γ_{RPG} factor for 937 nm and 30° is about half

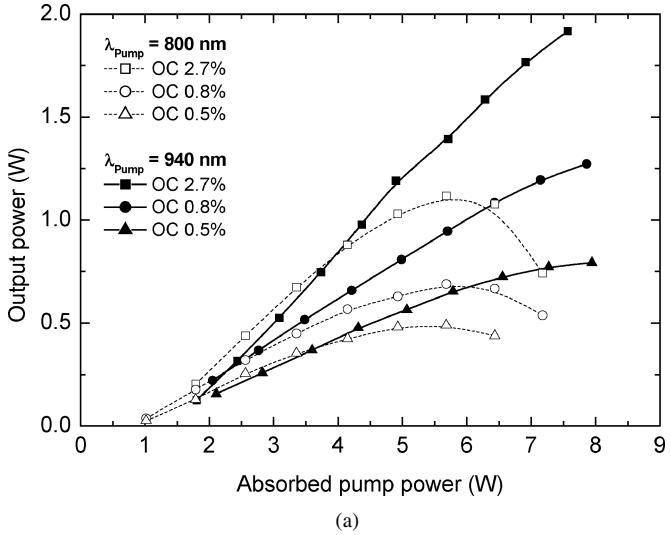

(a)

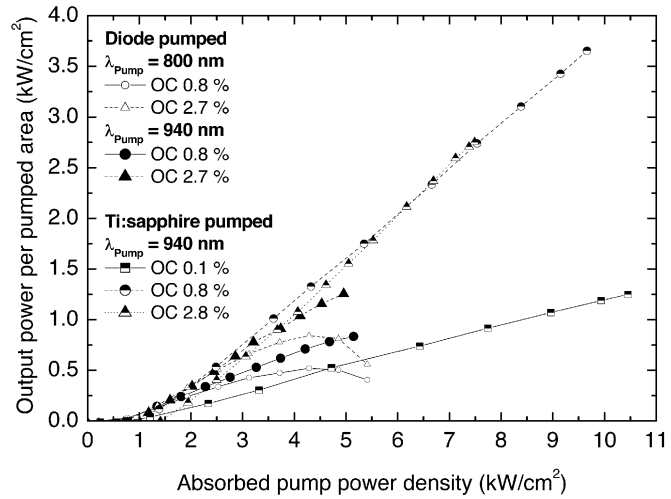

(b)

Fig. 10. (a) Laser output power as function of absorbed pump power for spacer (open symbols) and QW pumping (filled symbols) using the diode laser setups #2 and #3 and different out-coupling mirrors. For spacer pumping a thermal roll-over is visible. (b) Laser output power density as function of the absorbed pump power density for different out-coupling values. Shown are the results for Ti:sapphire pumping (setup #1, half-filled symbols) as well as diode pumping (setup #2 open and setup #3 filled symbols).

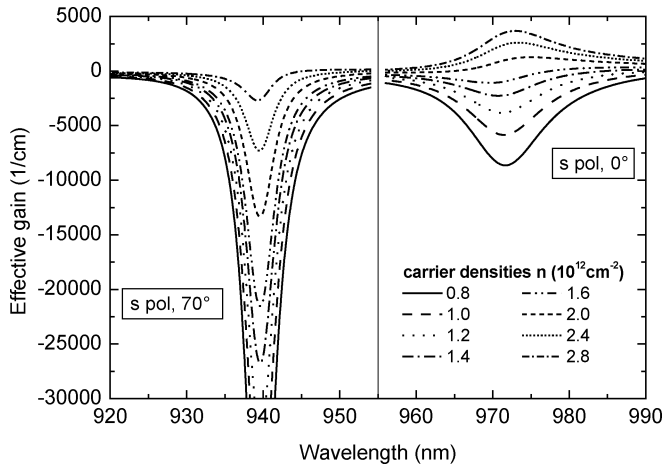

Fig. 11. Effective gain at 290 K, calculated with $g_{\mathrm{eff}} = \Gamma_{\mathrm{cav}} \cdot \Gamma_{\mathrm{RPG}} \cdot g_0$, for the Ti:sapphire experiments (setup #1) with the laser resonance at 972 nm. Parameter is the carrier density.

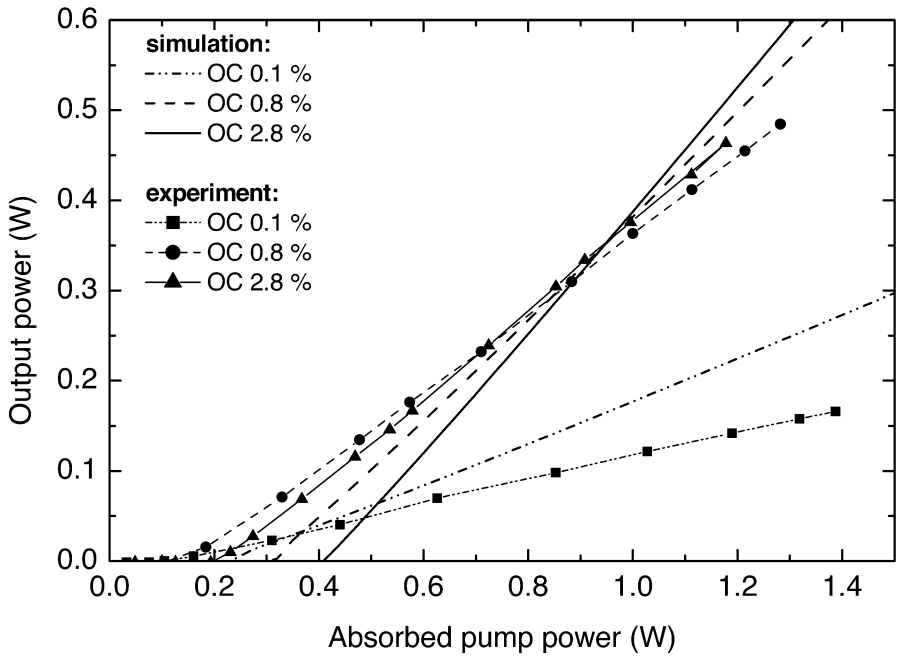

Fig. 12. Calculated $P_{\rm in}$ versus $P_{\rm out}$ curves for different out-coupling values (lines without symbols) shown together with the experimental ones obtained using in-well pumping at 940 nm using the Ti:sapphire pump laser setup #1 (lines with symbols).

way between the values for the 892 nm and the 940 nm Ti:sapphire pumped results. As can be seen in Fig. 10(b) the lasing threshold of QW and spacer pumping are similar and also comparable to the corresponding Ti:sapphire results. New, however, is the strong thermal roll-over of the high-power spacer-pumped output at absorbed pump powers of 5–7 W (4–5 kW/cm^2). Measuring the power dependent shift of the resonance lines (visible within the PL spectra) together with the corresponding temperature coefficient of 0.07 nm/K for the resonances gives an increase of the temperature of 11 K/Watt of absorbed pump power for spacer pumping. For QW pumping the increase in temperature due to pumping is measured to be 8 K/W.

4) Laser Modeling: As mentioned above, the calculated material gain/absorption spectra for various carrier densities and temperatures together with the spectroscopically determined Γ factors allow to calculate the effective (by cavity and RPG modified) gain/absorption spectra (Fig. 11). These data can be readily put into the simple rate equation model to simulate the laser behavior under various conditions and to compare the modeling results with the experimental results. For the simulations a heating coefficient of 10 K/W of absorbed pump power was assumed for our samples. This value originates from the measurements of the power dependent displacement of the resonance lines visible in the PL spectra recorded simultaneously with the power-in/power-out curves of our samples [4]. For Ti:sapphire experiments the internal loss L was determined to be about 0.2%. Pump wavelength was 940 nm and heat sink temperature 293 K. The Γ function was chosen corresponding to the pump spot position in the experiments. To account for the reduced differential efficiency as well as the absorption saturation behavior seen in the experiments $\eta_{\rm int}$ was set to 70% and $\eta_{\rm geo}$ to 80%. The so calculated output curves are shown in Fig. 12 together with the measured ones. The lasing wavelengths that result from the simulations are given in Table II alongside with the experimental values. As expected, the lasing wavelength is more strongly bound to the cavity resonance position at 972 nm for higher out-coupling values. The agreement between simulation and measurement for the different out-coupling values is remarkably good. Fig. 13 shows the calculated absorptance as function of the absorbed pump power which can be compared to the experimental results shown in Fig. 9. The decrease in pump absorption above lasing threshold is nicely reproduced, whereas the absolute absorptance values are slightly underestimated. However, one has to bear in mind the strong simplifications in the model made.

TABLE II
LASER WAVELENGTH AT MAXIMUM PUMP POWER USING TI:SAPPHIRE QW PUMPING FOR VARIOUS OUT-COUPLING VALUES OF THE EXTERNAL RESONATOR MIRROR

Out-coupling	Simulation	Experiment (Ti:sapphire)
0.06 %	997 nm	993 nm
0.8 %	985 nm	981 nm
1.5 %	978 nm	977 nm
2.8 %	974 nm	974 nm
5.7 %	973 nm	971 nm

For the diode pumped experiments the internal loss was set to 1.2%, which could be attributed to the larger pump spot size and the inhomogeneity of the samples. This manifests itself in the strong dependency of the differential efficiency on the out-coupling value as can be seen in the measurements. The intrinsic efficiency was set to 70% and the geometrical efficiency was set to 80%. Both, simulated and measured output curves are shown in Fig. 14. Again the agreement is within the scope of our simple model. The thermal roll-over for the calculated curves is not as

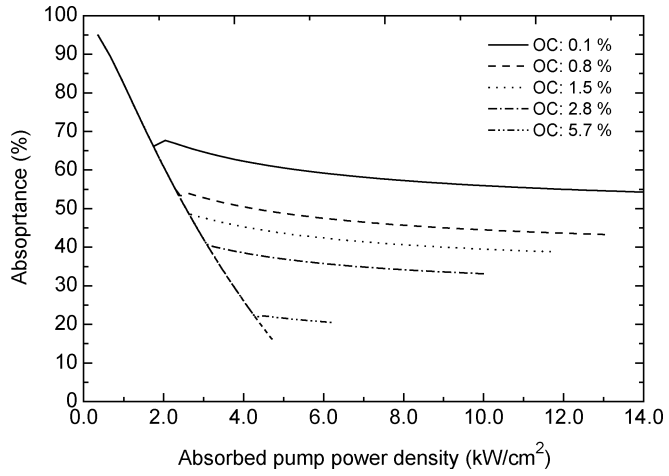

Fig. 13. Absorptance calculated for different out-coupling values and pumping at 70° with s polarized 940-nm radiation. The corresponding experimental results are shown in Fig. 9.

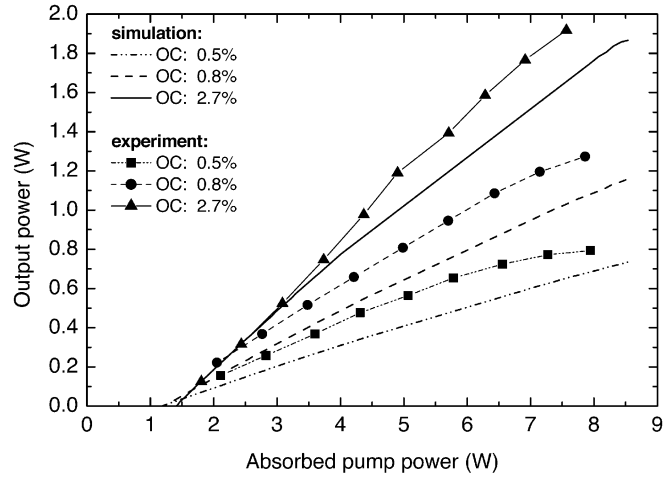

Fig. 14. Comparison of calculated (lines without symbols) and measured (lines with symbols) characteristic curve for diode in-well pumping with three different out-coupling values using setup #3.

pronounced as in the experimental curves. This could be a result of the constant heating rate assumed for the calculations. An increase of heating rate with temperature due to the increased threshold and Auger coefficient at higher temperatures is assumed to lead to a much faster thermal roll-over. Fig. 15 shows the calculated lasing wavelength as a function of absorbed pump power for three different out-coupling values and the experimental values for comparison. Both show the same tendency toward a shorter lasing wavelength for higher out-coupling values and a similar shift with absorbed power (indicating that the assumed T shift must be close to the real value).

IV. Discussion

Having included the geometry factor η_{geo} and the intrinsic efficiency η_{int} into the standard rate equations a good reproduction of the P_{out}-versus-P_{abs} curves could be achieved. They show an absorption threshold density of approx. 1 kW/cm^2 and a maximum slope efficiency of 50%. The saturation behavior of our samples is also well reproduced using our simple model.

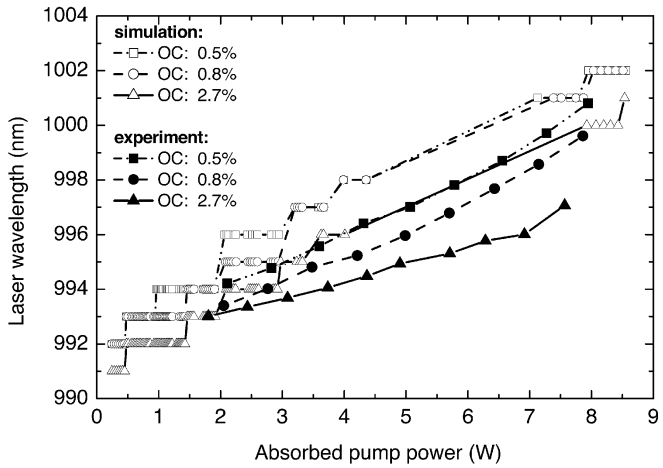

Fig. 15. Comparison of simulated lasing wavelength (open symbols) with the measured wavelengths (closed symbols) for different out-coupling values and diode in-well pumping using setup #3.

The limitation of the differential quantum efficiency to values below 55% for these samples indicates that the quantum defect may not be the only heat source within the active region. This can also be seen in the small difference of increase in temperature per Watt of absorbed power in the active region, which was measured to be 11 K/W for the spacer pumped case as compared to 8 K/W for the in-well pumped case. Nevertheless, no thermal roll-over was observed for QW pumping up to the maximum available pump power, which allowed to increase the maximum output power by 70% as compared to spacer pumping to 1.9 W, limited only by the available pump power.

From literature, it is well known that edge-emitting lasers as well as VCSELs are capable of intrinsic efficiencies close to 1 [22]. Since for optical pumping doping is not required such intrinsic efficiencies should be feasible with these optically pumped devices as well. In this case the advantage of in-well pumping for high output power systems should be even more pronounced.

Using low-brightness diode lasers for pumping in combination with an external multipass optics a reasonably good absorption efficiency of more than 60% could be achieved, despite the fact that the QW arrangement did not really fit to the pump field at 940 nm. Ways to increase the absorption efficiency are: 1) adjusting the cavity mode spacing to the pump-to-laser-wavelength difference and 2) optimizing the active region design to increase the RPG factor for pumping. A lasing wavelength of 985 nm and a pump wavelength of 940 nm at 35° of incidence leads to an optical cavity length of approximately 10 λ_{laser}, resulting in 20 antinodes of the laser field within the structure. To optimize the positioning of the QWs within the antinodes of pump and laser field only the first and the last 3 antinodes should be used. To get the same number of QWs as implemented in our sample, 2 QWs instead of one could be used per antinode of the field. This would result in an improved Γ factor of 6 for the pump radiation by simultaneously keeping the Γ factor of 7 for the laser radiation at 985 nm. This should give a nearly 6-fold improvement of the absorption in comparison to the above experiments using 13 QWs in a line, and should allow to reduce

the number of pump passes substantially from currently 12 to perhaps only 2 double passes.

In our experiments the quantum defect was reduced to values as low as 4%, leading to substantial bleaching of the pump transition. Choosing a pump wavelength of 915 nm instead of 940 nm can increase the intrinsic absorption from about 2600 cm^{-1} to 7200 cm^{-1} at $n = 1.5 \cdot 10^{12}$ cm^{-2}. In this case, a double-Bragg design with a slightly higher number of AlAs–GaAs pairs and a somewhat increased thermal resistance would be necessary. The double-pass absorption would then be increased from 26% to 56% giving an overall absorption of about 80% by simply redirecting the pump radiation onto the pump spot using a concave mirror. However, this comes at the cost of increased heating of the device and a tradeoff between ease of absorption and decrease of device temperature has to be made.

To fully use resonant absorption for in-well pumping a precise control of epitaxial growth and sample preparation is necessary. This is a direct result of the simultaneously fixed pump and lasing wavelength as compared to spacer pumping where the laser wavelength is fixed only. Due to the limited range of angles of incidence α between 30° and 50° when using highly divergent pump diodes the variation in allowed pump resonance position is only about 1%. The same allowance should be made for the lasing wavelength to limit the possible reduction of the RPG value. If more than two double passes are to be realized the allowed angle of incidence is usually even more restricted. For example using our conventional thin-disk multipass optic, α is limited to values between 27° and 37°, increasing the necessary accuracy in layer thickness to about 0.5%.

V. Summary

We have shown that with in-well pumping of semiconductor thin-disk lasers the usually thermally limited output power can be increased significantly due to a reduced heating of the active region. In our experiments an increase of output power by a factor of nearly 2 from 1.1 to 1.9 W was realized when changing the pump wavelength from 808 to 940 nm. The in-well pumped output power was limited by the available pump power rather than by thermal roll-over. These results are achieved without special heat-spreaders or particularly small pump spots to increase three dimensional heat flow. Therefore, this method can lead the way to true power scalability by simply increasing the pumped area and keeping constant the pump power density. The absorption efficiency is shown to be 60% in a first high-power diode-pumped experiment. Optimization of the device design should enable absorption efficiencies of better than 90%.

References

[1] A. Mooradian, "High brightness cavity-controlled surface emitting GaInAs lasers operating at 980 nm," in *Proc. OFC Tech. Dig. Postdeadline Papers*, 2001, pp. PD17-1–PD17-3.

[2] ——, "Overcoming hurdles on the road to more efficient diodes," *Photon. Spectra*, vol. 39, no. 2, pp. 59–60, Feb. 2005.

[3] M. Kuznetsov, F. Hakimi, R. Sprague, and A. Mooradian, "Design and characteristics of high power (0.5-W CW) diode-pumped vertical-external-cavity surface-emitting semiconductor lasers with circular TEM00 beams," *IEEE J. Sel. Topics Quantum Electron.*, vol. 5, pp. 561–573, May/Jun. 1999.

[4] S.-S. Beyertt, T. Kübler, U. Brauch, A. Giesen, E. Gerster, F. Rinaldi, and P. Unger, "Semiconductor thin disk laser-comparison of spacer and quantum-well pumping," in *Proc. Advanced Solid-State Photonics Topical Meeting*, Vienna, Austria, Feb. 2005, pp. MB35-1–MB35-3.

[5] S.-S. Beyertt, U. Brauch, A. Giesen, E. Gerster, and M. Zorn, "Direct pumping of quantum wells improves performance of semiconductor thin-disk lasers," *Photon. Spectra*, vol. 39, no. 6, pp. 60–66, Jun. 2005.

[6] A. Giesen, S.-S. Beyertt, and U. Brauch, "Laser amplifier system," EU Patent Application WO 03/100 922 A2, May 20, 2003.

[7] M. I. Müller, C. Karnutsch, J. Luft, W. Schmid, K. Streubel, N. Linder, S.-S. Beyertt, U. Brauch, A. Giesen, and G. H. Döhler, "Optically pumped vertical external cavity semiconductor thin-disk laser with CW operation at 660 nm," in *Proc. Int. Symp. Compound Semiconductors*, vol. 174, 2003, pp. 427–430.

[8] A. Giesen, "Results and scaling laws of thin-disk lasers," *Proc. SPIE Solid State Lasers XIII: Technology and Devices*, vol. 5332, pp. 212–227, 2004.

[9] M. I. Müller, "Optisch gepumpte oberflächenemittierende Halbleiterlaser mit externem Resonator für 650 nm auf der Basis von InGaAlP," in *Physik Mikrostrukturierter Halbleiter*, S. Malzer, T. Marek, and P. Kiesel, Eds. Erlangen-Nürnberg, Germany: Lehrstuhl für Mikrocharakterisierung, Friedrich-Alexander-Universität.

[10] M. Schmid, S. Benchabane, F. Torabi-Goudarzi, R. Abram, A. I. Ferguson, and E. Riis, "Optical in-well pumping of a vertical-external-cavity surface-emitting laser," *Appl. Phys. Lett.*, vol. 84, pp. 4860–4862, Jun. 2004.

[11] A. Giesen, H. Hügel, A. Voss, K. Wittig, U. Brauch, and H. Opower, "Scalable concept for diode-pumped high-power solid-state lasers," *Appl. Phys. B: Lasers Opt.*, vol. B58, pp. 365–372, 1994.

[12] A. P. Ongstad, M. L. Tilton, E. J. Bochove, and G. C. Dente, "Carrier spillover at 300, 195, and 77 K in InGaAs and GaAs single quantum wells," *J. Appl. Phys.*, vol. 80, pp. 2866–2872, Sep. 1996.

[13] U. Strauss, W. W. Rühle, and K. Köhler, "Auger recombination in intrinsic GaAs," *Appl. Phys. Let.t*, vol. 62, pp. 55–57, Jan. 1993.

[14] H. Wenzel, G. Erbert, and P. Enders, "Improved theory of the refractive-index change in quantum-well lasers," *IEEE J. Sel. Topics Quantum Electron.*, vol. 5, no. 3, pp. 637–642, May/Jun. 1999.

[15] A. P. Bogatov, A. E. Drakin, D. V. Batrak, R. Güther, K. Paschke, and H. Wenzel, "Spectral selectivity of a αDFB semiconductor laser cavity," *Quantum Electron.*, submitted for publication.

[16] R. Michalzik and K. J. Ebeling, "Operating principle of VCSELs," in *Vertical-Cavity-Surface-Emitting-Laser Device*, H. E. Li and K. Iga, Eds. Berlin, Germany: Springer-Verlag, 2003, vol. 6, ch. 3, pp. 53–98.

[17] E. M. Purcell, "Spontaneous emission probabilities at radio frequencies," *Phys. Rev.*, vol. 69, p. 681, Jun. 1946.

[18] C. Wilmsen, H. Temkin, and L. A. Coldren, *Vertical-Cavity Surface-Emitting Lasers: Design, Fabrication, Characterization, and Applications*. Cambridge, U.K.: Cambridge Univ. Press, 1999.

[19] F. Bugge, U. Zeimer, H. Wenzel, G. Erbert, and M. Weyers, "Interdiffusion in highly strained InGaAs-QWs for high power laser diode applications," *J. Cryst. Growth*, vol. 272, pp. 531–537, Dec. 2004.

[20] W. Pittroff, G. Erbert, G. Beister, F. Bugge, A. Klein, A. Knauer, J. Maege, P. Ressel, J. Sebastian, R. Staske, and G. Traenkle, "Mounting of high power laser diodes on boron nitride heat sinks using an optimized Au/Sn metallurgy," *IEEE Trans. Adv. Packag.*, vol. 24, no. 4, pp. 434–441, Nov. 2001.

[21] J. Geske, K.-G. Gan, Y. L. Okuno, J. Piprek, and J. E. Bowers, "Vertical-cavity surface-emitting laser active regions for enhanced performance with optical pumping," *IEEE J. Quantum Electron.*, vol. 40, no. 9, pp. 1155–1162, Sep. 2004.

[22] R. Jäger, M. Grabherr, C. Jung, R. Michalzik, G. Reiner, B. Weigl, and K. J. Ebeling, "57% wallplug efficiency oxide-confined 850 nm wavelength GaAs VCSELs," *Electron. Lett.*, vol. 33, pp. 330–331, 1997.

Svent-Simon Beyertt was born in Schorndorf, Germany. He received the diploma in physics from Eberhard Karls Universität, Tübingen, Germany, in 2000. He is currently working toward the Ph.D. degree at the University of Stuttgart, Stuttgart, Germany, with interest focused on semiconductor thin-disk lasers.

Mr. Beyertt is a member of the German Physical Society.

Martin Zorn was born in Berlin, Germany, in 1967. He received the diploma in physics and the Ph.D. degree also in physics from the Technical University of Berlin, Berlin, Germany, in 1994 and 1999, respectively.

In 1999, he joined the Ferdinand-Braun-Institut für Höchstfrequenztechnik (FBH), Berlin, Germany, and is presently working in the field of epitaxy for edge-emitting and surface-emitting laser diodes using metalorganic vapor phase epitaxy (MOVPE).

Dr. Zorn is a member of the German Physical Society.

Thomas Kübler was born in Ludwigsburg, Germany. He received the diploma in physics from University of Stuttgart, Stuttgart, Germany, in 2000. He is currently working toward the Ph.D. at the University of Stuttgart, with focus on modeling semiconductor thin-disk-lasers.

From 2000 to 2002, he worked on pattern-formation in water-jet cutting processes at the University of Stuttgart and the University of Münster, Münster, Germany.

Mr. Kübler is a member of the German Physical Society.

Hans Wenzel was born in Sonneberg, Germany, in 1960. He received the diploma and the Ph.D. degrees in physics from Humboldt University, Berlin, Germany, in 1986 and 1991, respectively.

From 1991 to 1994, he has been involved in a research project on the modeling of DFB lasers at Humboldt University. In 1992, he was with TFL Telecommunications Research Laboratory, Hjrsholm, Denmark, for three months. In 1994, he joined the Ferdinand-Braun-Institut für Höchstfrequenztechnik (FBH), Berlin, Germany, where he is currently working on the simulation of high-power lasers. His present research interests include VCSELs and QW lasers.

Dr. Wenzel is a member of the German Physical Society.

Markus Weyers received the diploma in physics and the Dr.rer.nat. degree from RWTH Aachen, Germany, in 1986 and 1990, respectively, where he worked on basic growth studies in MOMBE.

From September 1990 to March 1992, he was with NTT Basic Research Laboratories, Musashino, Japan, where he worked on growth mechanisms of GaAs and GaP in MOVPE and was the first to study growth and properties of GaAsN. Since April 1992, he has been Head of the Materials Technology Department at Ferdinand-Braun-Institut für Höchstfrequenztechnik, Berlin, Germany. His research interests include growth of GaAs-based laser structures as well as HBTs and also GaN growth by HVPE.

Adolf Giesen was born in 1946. He received the diploma in physics and the Ph.D. degree from the University of Bonn, Bonn, Germany.

In 1982, he joined the DLR (German Aerospace Establishment) working on RF-excited CO_2-laser development and characterization of optical components under high-power irradiation. Since 1986, he has been Head of the Laser Development and Laser Optics Department of the Institut für Strahlwerkzeuge (IFSW), University of Stuttgart, Stuttgart, Germany. His work is concentrated on thin disc lasers, phase coupling of diode lasers, and characterization of laser beams and of optical components.

Günther Tränkle (M'95) received the diploma in physics from the Technical University (TU) of Germany, Munich, in 1981 and the Ph.D. degree in physics from the University of Stuttgart, Stuttgart, Germany, in 1988, where he worked on quantization and many-body effects in III–V quantum-well structures.

In 1988, he joined the Walter-Schottky Institute at TU Munich, running its III–V semiconductor technology and working on field-effect transistors and laser diodes. From 1995 to 1996, he was a Department Head at the Fraunhofer-Institute for Applied Solid-State Physics, Freiburg, Germany, and was responsible for the development and realization of electronic and optoelectronic III-V semiconductor devices, as well as quantum-well infrared detector arrays. In August 1996, he became Head of the Ferdinand-Braun-Institut für Höchstfrequenztechnik, Berlin, Germany. From 1999 to 2000, he was Chairman of the Forschungsverbund Berlin. His current research interests include GaAs technology, micro- and millimeter-wave transistors and circuits, GaN electronics, and high-power diode lasers.

Uwe Brauch was born in 1958. He received the diploma degree in physics and the Ph.D. degree from the University of Stuttgart, Stuttgart, Germany, in 1983 and 1986, respectively, where he worked on new tunable lasers based on fluoride crystals.

The following year, he was with Fibertek, Inc., Herndon, VA, applying the laser-heated pedestal growth method to explore new laser crystals. In 1987, he joined the DFVLR, Stuttgart (now DLR, German Aerospace Center) where he was involved in solar- and diode-pumped lasers, coherent coupling of diode lasers, and the application of lasers in fields like crystal growth, displays, and photo-lithography. Since 2002, he has been with the Institut für Strahlwerkzeuge (IFSW), University of Stuttgart. His current research is focused on semiconductor thin-disk lasers.